Atmos. Chem. Phys. Discuss., 14, 28203–28230, 2014
www.atmos-chem-phys-discuss.net/14/28203/2014/
doi:10.5194/acpd-14-28203-2014

Atmospheric Chemistry and Physics Discussions

Variability of Antarctic ozone loss in the last decade (2004–2013): high resolution simulations compared to Aura MLS observations

J. Kuttippurath[1], S. Godin-Beekmann[1], F. Lefèvre[1], M. L. Santee[2], L. Froidevaux[2], and A. Hauchecorne[1]

[1]UPMC Université de Paris 06, UMR8190 LATMOS-IPSL, CNRS/INSU, 75005 Paris, France
[2]JPL/NASA, California Institute of Technology, Pasadena, California, USA

Received: 29 September 2014 – Accepted: 27 October 2014 – Published: 13 November 2014

Correspondence to: J. Kuttippurath (jayan@latmos.ipsl.fr)

Published by Copernicus Publications on behalf of the European Geosciences Union.

Abstract

A detailed analysis of the polar ozone loss processes during ten recent Antarctic winters is presented with high resolution Mimosa-Chim model simulations and high frequency polar vortex observations from the Aura Microwave Limb Sounder (MLS) instrument. Our model results for the Antarctic winters 2004–2013 show that chemical ozone loss starts in the edge region of the vortex at equivalent latitudes (EqLs) of 65–69° S in mid-June/July. The loss progresses with time at higher EqLs and intensifies during August–September over the range 400–600 K. The loss peaks in late September/early October, where all EqLs (65–83°) show similar loss and the maximum loss (> 2 ppmv [parts per million by volume]) is found over a broad vertical range of 475–550 K. In the lower stratosphere, most winters show similar ozone loss and production rates. In general, at 500 K, the loss rates are about 2–3 ppbv sh^{-1} (parts per billion by volume/sunlit hour) in July and 4–5 ppbv sh^{-1} in August/mid-September, while they drop rapidly to zero by late September. In the middle stratosphere, the loss rates are about 3–5 ppbv sh^{-1} in July–August and October at 675 K. It is found that the Antarctic ozone hole (June–September) is controlled by the halogen cycles at about 90–95 % (ClO–ClO, BrO–ClO, and ClO–O) and the loss above 700 K is dominated by the NO_x cycle at about 70–75 %. On average, the Mimosa-Chim simulations show that the very cold winters of 2005 and 2006 exhibit a maximum loss of ∼ 3.5 ppmv around 550 K or about 149–173 DU over 350–850 K and the warmer winters of 2004, 2010, and 2012 show a loss of ∼2.6 ppmv around 475–500 K or 131–154 DU over 350–850 K. The winters of 2007, 2008, and 2011 were moderately cold and thus both ozone loss and peak loss altitudes are between these two ranges (3 ppmv around 500 K or 150 ± 10 DU). The modeled ozone loss values are in reasonably good agreement with those estimated from Aura MLS measurements, but the model underestimates the observed ClO, largely due to the slower vertical descent in the model during spring.

ACPD
14, 28203–28230, 2014

1 Introduction

Large variability in Antarctic ozone loss has been seen in the last few years (2004–2013) relative to other winters since 1992 (e.g. Tilmes et al., 2006; Huck et al., 2007; Yang et al., 2006; Santee et al., 2008a). For instance, the winters 2004, 2010, and 2012 were relatively warm with minor warmings and hence, limited ozone loss (Santee et al., 2005; de Laat and van Weele, 2011). The first fortnight of August 2005 was unusually cold and showed a high rate of ozone loss and an unprecedented ozone hole (WMO, 2011). The winter of 2006 was one of the coldest and hence, the Antartic vortex experienced the largest ozone hole to date (Santee et al., 2011; WMO, 2011). The winters 2007, 2009, and 2013 were characterized by average temperatures and hence, ozone holes of moderate size (Tully et al., 2008; Kuttippurath et al., 2013). However, the winters 2008 and 2011 were again very cold and characterized by large ozone holes (Tully et al., 2011; WMO, 2011). Here, we provide a detailed view of these ten winters in relation to polar processing and the chemistry of ozone loss.

In this study, we discuss (i) the interannual variability of ozone loss and chlorine activation, (ii) horizontal, vertical, and seasonal variability of ozone loss, and (iii) contributions of various chemical cycles to the ozone loss in the Antarctic stratosphere during these winters. Additionally, the past ten winters offer a good opportunity to test the chemical and dynamical processes in numerical models. Furthermore, the Aura Microwave Limb Sounder (MLS) observations (Froidevaux et al., 2008; Santee et al., 2008b), one of the best satellite instruments currently available for sampling polar vortices, are compared to the model results. Therefore, for the first time ozone loss and chlorine activation can be studied with such high resolution measurements with high spatial and temporal coverage inside the Antarctic vortex. Previous satellite measurements were relatively limited to a small temporal and spatial area as far as high latitude observations are concerned (e.g. Tilmes et al., 2006; Hoppel et al., 2005). While the Upper Atmosphere Research Satellite MLS had a similar latitudinal coverage, the frequency of its polar measurements was lower than that of Aura MLS (e.g. Waters et al.,

ACPD
14, 28203–28230, 2014

1999). Therefore, this study offers some new insights on the polar processing and ozone loss features of the Antarctic stratosphere.

In this article, the Mimosa-Chim model is used to simulate the chemical constituents for the period 2004–2013. The simulated results are then compared to the Aura MLS measurements. We first look at the average ozone loss evolution within different equivalent latitudes (EqLs) in Sect. 3.1. The vertical distribution of the contribution of various chemical cycles to the ozone loss in the stratosphere is discussed in Sect. 3.2. The assessment of the interannual variability of the ozone loss, chlorine activation, and ozone loss rates during the ten (2004–2013) winters is presented in Sect. 3.3. Finally, Sect. 4 concludes with our main findings.

2 Simulations and measurements

We use the high resolution Mimosa-Chim chemical transport model (CTM) for the simulations of chemical constituents (e.g. Kuttippurath et al., 2010; Tripathi et al., 2007). The model extends horizontally from 10° N to 90° S with 1° × 1° resolution and there are 25 isentropic vertical levels between 350 and 950 K with a resolution of about 1.5–2 km. The model is forced by European Centre for Medium-Range Weather Forecasts (ECMWF) analyses. Chemical fields in the model are initialized from the 3-D CTM REPROBUS output (Lefèvre et al., 1994) and it uses the MIDRAD radiation scheme (Shine, 1987). Climatological H_2O, CO_2, but interactive O_3 fields are used for the calculation of heating rates. The kinetics data are taken from Sander et al. (2011), but the Cl_2O_2 photolysis cross-sections from Burkholder et al. (1990), with a log-linear extrapolation up to 450 nm (Stimpfle et al., 2004). These cross-sections are in good agreement with the recent Cl_2O_2 measurements by Papanastasiou et al. (2009), which form the basis for the JPL 2011 recommendations (i.e. Sander et al., 2011). For each Antarctic winter the model was run from 1 May to 31 October.

The model has detailed polar stratospheric cloud (PSC) formation and growth and sedimentation schemes. The saturation vapor pressure provided by Hanson and

ACPD
14, 28203–28230, 2014

Mauersberger (1988) and Murray (1967) is used to assume the existence of Nitric Acid Trihydrate (NAT) and ice particles, respectively. Liquid supercooled sulphuric acid aerosols, NAT, and ice particles are considered in equilibrium with the gas phase (Lefèvre et al., 1998). Equilibrium composition and volume of binary (H_2SO_4–H_2O) and ternary (HNO_3–H_2SO_4–H_2O) droplets are calculated using an analytic expression given by Carslaw et al. (1995). For NAT and ice particles, the number density is set to 5×10^{-3} cm^{-3} and the particle diameter is calculated within the scheme, from the available volume of HNO_3 and H_2SO. In the denitrification module, the sedimentation of HNO_3 containing particles where the NAT particles are assumed to be in equilibrium with gas phase HNO_3. All the three types of NAT, ice, and liquid aerosols particles are considered and the sedimentation speed of the particles is calculated according to Pruppacher and Klett (2010).

We use the Aura MLS measurements version (v) 3.3 to compare with simulations. The ozone measurements have a vertical resolution of 2.5–3 km over 215–0.02 hPa and the vertical resolution of ClO measurements is about 3–3.5 km over 100–1 hPa. The estimated uncertainty of typical ozone and ClO retrievals is about 5–10 and 10–20 %, respectively (Livesey et al., 2011; Santee et al., 2011, 2008a; Froidevaux et al., 2008). To compare with the measurements, the model results (6 h output) are interpolated to the measurement locations with respect to the time of measurements.

3 Results and discussion

3.1 Ozone loss: the 2004–2013 average

To elucidate various chemical ozone loss features, we analyze the vertical distribution of the average loss in 2004–2013 for different EqL bins estimated from the model and MLS data from May to October, and shown in Fig. 1. The EqL-based analyses extend from 65 to 83° S in 2° increments as calculated for the MLS measurements. A detailed discussion on the calculation of EqLs and determination of the polar vortex edge can

ACPD
14, 28203–28230, 2014

be found in Nash et al. (1996) and references therein. The simulations show that the chemical loss (passive ozone minus ozone) starts at lower EqLs of 65–67° S at the edge of the Antarctic vortex in June, above 600 K, as also shown by Lee et al. (2000) and Roscoe et al. (2012). It moves down to the lower altitudes by July and the loss is largest at 65–69° S EqL. The loss increases again in August, with the EqLs of 65 and 83° S showing the largest and smallest loss, respectively, in accordance with the increase in incidence of sunlight over the region. A clear difference in the amount of ozone loss estimated at different EqLs is well simulated. At the edge of the vortex, maximum modeled ozone loss of 2.1 ppmv (parts per million by volume) is found around 500 K, while in the 70–80° S EqL range the peak loss is found above 600 K.

The ozone loss continues through to September, when all EqLs show very large loss. The largest modeled loss is still found in the lower EqLs of 65–69° S, reaching about 3 ppmv at 500 K. The higher EqLs (75–83° S) show the smallest ozone loss and it peaks in the middle stratosphere while other EqLs show their peak loss in the lower stratosphere, below 575 K. Above 600 K, all EqLs show similar ozone loss of about 1.4 ppmv. The maximum loss is about 3 ppmv at 65–70° S at 500 K, 2.5 ppmv at 70–75° S at 550 K, 1.7 ppmv at 75–80° S at 575 K, and 1.3 ppmv over 80–83° S at 600 K, and thus, the altitude of maximum loss increases with EqL up to September. As expected, the maximum ozone loss is found in October, and all EqLs show more or less the same loss (about 3 ppmv) at the peak loss altitude of around 500 K. In addition, all EqLs show ozone losses below 500 K that are about the same as at 500 K. Above 500 K, the ozone loss shows slight differences, with the largest loss occurring at the highest EqLs, unlike in months earlier than September. Note that the ozone loss presented here is the cumulative ozone loss, not the instantaneous loss (see later analyses), which explains the large ozone loss estimated for late September and October after the normal chlorine activation period.

The analyses with model results are in good agreement with those of the MLS measurements (passive ozone minus MLS ozone). Nevertheless, the loss estimated from the observations is more compact with altitude in October, and the

ACPD
14, 28203–28230, 2014

model–measurement differences are relatively larger in September. The comparison of ozone loss above 550 K shows that the model overestimates the ozone loss there. The ozone loss deduced from the measurements at 360–370 K in May is insignificant (about 0.05–0.08 ppmv), and is within the estimated error bars of the measurements. The differences between measurements and simulations will be discussed further in Sect. 3.3.1.

3.2 Chemical cycles: the 2004–2013 average

In this section, we make a comprehensive analysis of the mean contributions of various chemical cycles to the ozone loss in 2004–2013. The instantaneous contribution (ppbv sh^{-1}) of the five important chemical cycles is presented in Fig. 2. Further details and reaction sequences of the ozone loss cycles are given in Table 1. In the lower stratosphere (below 550 K), about 90 % of ozone loss is controlled by the ClO–ClO and BrO–ClO cycles from June to September with a maximum of about 0.5 ppbv sh^{-1} in August and September. The ClO–ClO cycle is more important than the latter cycle, as the contribution from the latter cycle hardly exceeds 0.3 ppbv sh^{-1}. A constant contribution of about 0.1–0.2 ppbv sh^{-1} (5–10 %) from the ClO–O cycle is also evident from June to September in the lower stratosphere (at 450–500 K). Above 550 K, the contribution from NO_x dominates in spring while ClO–O dominates in winter, with about 2–3 ppbv sh^{-1} (see the black contour lines) and 0.4–0.5 ppbv sh^{-1}, respectively, depending on the day of the year. The contribution from the HO_x cycle is negligible during the ozone hole period, as it is significant only in late October at altitudes above 700 K. Contributions of these cycles principally depend on the available O-atoms, as the rate limiting step of these cycles is the combination of a specific molecule with the O atom (e.g. see Table 1). These analyses show that the Antarctic ozone hole is primarily controlled by the halogen cycles in tune with previous findings (e.g. WMO, 2011 and references therein) and the magnitude of loss above 700 K depends on the amount of O-atoms, dynamics, and the availability of NO_x in each winter.

ACPD
14, 28203–28230, 2014

3.3 Interannual variations

We have already discussed the general features of ozone loss evolution and related chemical cycles in the Antarctic stratosphere. Now we discuss the interannual variations in chlorine activation, ozone loss, and ozone production and loss rates during 2004–2013.

3.3.1 Chlorine activation

Figure 3 compares the simulated and measured ClO at the MLS sampling points inside the vortex, defined here by the area within 65–90° S EqL, and with solar zenith angle (SZA) less than 89° as available, for the Antarctic winters 2004–2013. In Mimosa-Chim, relatively high chlorine activation is found in 2005, when a maximum of 1.6–1.8 ppbv (parts per billion by volume) is simulated from June to late July and early August, consistent with the lower temperatures in that winter (WMO, 2011). The other winters show a more or less similar distribution of ClO and thus, chlorine activation, except in the warm winters of 2010 and 2012. The simulated ClO stands in contrast to the temperature structure and PSC observations in each winter (Pitts et al., 2009), which showed the largest areas of PSCs in the coldest winters of 2005 and 2006. However, when we examine the MLS measurements, they mostly follow the temperature history of each winter, as the observations show the strongest chlorine activation in 2005 and 2006, and the weakest in 2010 and 2012. The highest ClO values (> 1.5 ppbv) are found from July to the end of September over 450–600 K in the colder winters, but around 550 K episodically in July–August in the warmer winters in the observations. Therefore, in contrast to the model results, the vortex averaged MLS observations display a clear interannual variation in the chlorine activation. These comparisons show that the model underestimates the observed ClO over 450–600 K.

In order to find out the reasons for the differences between simulated and measured ClO, we compared the simulated HCl, N_2O, and HNO_3 with the MLS observations. Figure 4 illustrates the ten year average of the vortex mean (defined by ≥ 65° EqL) ClO,

ACPD
14, 28203–28230, 2014

HCl, N_2O, HNO_3, O_3 and ozone loss from the Mimosa-Chim model and MLS measurements. The N_2O comparisons show that the simulations are higher than the measurements, as illustrated by the 50 and 100 ppbv isopleths. This bias in the simulations implies that the vertical diabatic descent in the model is slower than that deduced from MLS observations in polar spring. Consequently, the Cl_y (and thus ClO) and ozone in the model are relatively lower. Both HCl and ozone comparisons corroborate this feature of the simulations, as the HCl values are higher (0.5 ppbv), and ozone and ClO are lower (about 0.5 ppmv of O_3 and 0.3–0.5 ppbv of ClO) in the model calculations in spring. Therefore, we applied the Cl_2O_2 recombination rate constant of Nickolaisen et al. (2006) instead of the JPL recommendation, as suggested by von Hobe et al. (2007). However, the ClO results did not improve significantly and hence, the original simulations are presented. The HNO_3 comparisons also point out that the denitrification in the model is overestimated.

Note that the relatively low model top could also influence the slower descent or vertical transport in the model (a detailed discussion on this subject is a future work). Also, there can be small interannual differences in the diabatic descent, depending on the accuracy of the wind fields. These have to be kept in mind while interpreting the simulations. However, in a similar study, Santee et al. (2008a) compared the MLS measurements to SLIMCAT model results and found that their simulations slightly overestimate the ClO measurements for the Antarctic winters 2004 and 2005. They attributed these differences to the equilibrium PSC scheme of the model. In contrast, our model ClO results underestimate the observations, although using a very similar PSC scheme in the model. It suggests that even if the models use similar PSC schemes, the difference in model dynamics can induce significant changes in the simulated results. Nevertheless, note that the model has performed better in northern hemispheric simulations, where the ClO simulations overestimate the MLS measurements in the 2011 winter (Kuttippurath et al., 2012), but slightly underestimate them in 2005–2010 (Kuttippurath et al., 2010). This discrepancy in the simulations suggests that good representation of vertical transport in most CTMs is still a critical issue.

ACPD
14, 28203–28230, 2014

3.3.2 Ozone loss: vertical and temporal features

Figure 5 shows the vortex averaged ozone loss estimated from the model and MLS at the MLS sampling locations inside the vortex in 2004–2013. As discussed in Sect. 3.1, the ozone loss onset in the model occurs in mid-June at altitudes above 550 K and gradually moves down to the lower stratosphere by mid-August. The loss intensifies by mid-August, peaks by late September/early October and slows down thereafter as the ozone recovers through dynamical processes.

In the simulations, as expected, the colder winters of 2005 and 2006 show early onset of ozone loss, in mid-June. The estimated loss is less than 0.5 ppmv above 675 K until mid-August, increases to 1–1.5 ppmv by mid-September in the lower stratosphere, and peaks at 2.5–3.6 ppmv over 450–600 K by early October, consistent with the temporal and vertical extent of activated ClO in these winters. A maximum ozone loss of around 3.5 ppmv is derived around 550 K in 2005–2006 and about 3 ppmv around 500 K in 2007, 2008 and 2011. Relatively smaller ozone loss is found in the warmer winters of 2004, 2010 and 2012, where the peak loss is about 2.6 ppmv, around 475 K. A similar range of ozone loss, but in a slightly broader vertical extent of 450–600 K, is simulated in 2009 and 2013. Therefore, the center of the peak ozone loss altitude (i.e. loss > 2 ppmv) also shows corresponding variations in agreement with the meteorology of the winters, as it is located around 550 K in very cold winters (e.g. 2005 and 2006), around 500 K in moderately cold winters (e.g. 2007), and around 475 K in warm winters (e.g. 2004 and 2012).

In general, the timing and vertical range of ozone loss in the simulations are similar to those of the observations. The modeled ozone loss onset is in mid-June, except for the colder winters (when it is in mid-May), as discussed previously, and the loss strengthens by August–September and reaches a maximum in early to mid-October, consistent with those of the observations. The large ozone losses observed above 550 K in September–October in the colder winters are also reproduced by the model. However, the model consistently overestimates the measured ozone loss (i.e. passive ozone mi-

ACPD
14, 28203–28230, 2014

nus the MLS ozone) in the middle stratosphere in all years by about 0.2–0.5 ppmv in spring, as the model underestimates the measured ozone by the same amount at these altitudes, primarily due to the slower descent in the model during the period as discussed before (see previous discussion). Also, for the same reasons, the modeled loss exceeds that inferred from the measurements in some winters (e.g. 2005, 2010, and 2011) but is less in others (e.g. 2006 and 2007). Both the simulations and the measurements, however, provide consistent results for the peak ozone loss altitudes in each winter.

The ozone loss derived from the SCanning Imaging Absorption spectroMeter for Atmospheric CHartographY (SCIAMACHY) ozone profiles using the vortex descent method shows comparable values to that of the simulations/MLS data for the Antarctic winters 2004–2008 (Sonkaew et al., 2013). There is also good agreement in peak ozone loss values (around 3–3.5 ppmv) and the differences in the altitudes of maximum loss for various winters, as discussed previously for the modeled/MLS ozone loss. In addition, the large loss above 500 K found in the model/MLS data is also inferred from the SCIAMACHY measurements.

3.3.3 Partial column ozone loss

We have also calculated the column ozone loss from the simulations and observations at the MLS footprints inside the vortex for each winter for the complete altitude range of the model and for the altitude region over which peak loss occurs (400–600 K); results are given in Table 2. The simulated results show the lowest ozone loss in 2004 and the highest in 2005 at 350–850 K, consistent with the meteorology and chlorine activation during the winters. However, it has to be noted that the ozone hole in 2006 was record-breaking, but the model simulations show slightly lower total column ozone loss compared to 2005, due to the comparatively larger chlorine activation in early winter in 2005, as also illustrated in Fig. 3 (see the difference in chlorine activation in 2006 and 2005). Large ozone loss of about 167 DU is also simulated in the winter 2007 due to relatively strong chlorine activation in that winter (Fig. 3). The other winters

ACPD
14, 28203–28230, 2014

show a column ozone loss of about 155 ± 10 DU over the same altitude range. On the other hand, the ozone loss derived from MLS observations (passive ozone minus MLS ozone) shows the highest column ozone loss of about 162–166 DU in the very cold winters of 2005 and 2006, and the lowest of around 127–134 DU in the moderately cold winter of 2013 and the warm winters of 2010 and 2012 at 350–850 K, and these are in agreement with the meteorology of the winters. Despite the differences in the values, the ozone column loss computed for 400–600 K also shows similar patterns as those discussed for the 350–850 K range. Note that there was strong and prolonged chlorine activation in the coldest winter 2006 (i.e. ClO was enhanced slightly longer in this winter than in most other winters). Also, Santee et al. (2011) showed that there was unusually strong chlorine activation in the lowermost stratosphere (around 375 K) that contributed to the record-setting ozone hole/loss in that winter. Therefore, the data exhibit a clear interannual variation of ozone column loss as discussed for the ozone loss profile comparisons in Sect. 3.3.2.

The average partial column ozone depletion above the 550 K level computed from the model and data for the ten winters is about 50±5 DU. This column ozone loss has to be considered when deriving partial column loss from profiles. This is slightly different from the Arctic, where significant ozone loss occurs mostly in the lower stratosphere over 350–550 K in colder winters, and where the depletion above 550 K is limited to ~ 19±7 DU (Kuttippurath et al., 2010). The relatively larger Antarctic ozone column loss contribution from higher altitudes (above 550 K) is consistent with the loss estimated above those altitudes, as shown by the ozone profiles in this study for 2004–2013, and in Lemmen et al. (2006) and Hoppel et al. (2005) for a range of Antarctic winters prior to 2004. It is also evident from the maximum ozone loss altitudes, as most Antarctic winters have their peak loss altitudes around 550 K as opposed to 475 K in the Arctic (e.g. Kuttippurath et al., 2012; Tripathi et al., 2007; Grooß et al., 2005b; Rex et al., 2004).

The partial column loss estimated from the Halogen Occultation Experiment ozone measurements (~ 172 DU) over 350–600 K (Tilmes et al., 2006) is larger than our re-

ACPD
14, 28203–28230, 2014

sults for 2004. Our loss estimates over 350–850 K for 2004–2010 are in reasonable agreement with those derived from ground-based and other satellite total ozone observations in the Antarctic (Kuttippurath et al., 2013). The ozone loss computed from a bias-corrected satellite data set using a parameterized tracer by Huck et al. (2007) for the winter 2004 also shows a similar estimate. The slight differences amongst various ozone loss values can be due to the differences in the altitude of ozone loss estimates, vortex definition, vortex sampling, and the method used to quantify the loss by the respective studies.

3.3.4 Ozone loss and production rates

The interannual variability of ozone loss is further analyzed with the ozone loss and production rates. Figure 6 shows the instantaneous loss and production rates at 675 and 500 K. In general, at 500 K, the loss rates are about 2–3 ppbv sh^{-1} (ppbv/sunlit hour) in mid-June during the onset of ozone loss, about 3–4 ppbv sh^{-1} in July as the loss advances to the vortex core, and about 4–5 ppbv sh^{-1} from August to mid-September during the peak loss period. The loss rates decrease from late September onward and reach zero by mid-October, and stay at near-zero values thereafter. Since the loss rate during the mid-September to October period depends on natural ozone production and loss, interannual variability is small in that period, and most winters show loss rates of about 2–5 ppbv sh^{-1}. However, significant year-to-year variations are noted from mid-June to mid-August, as the loss rate depends on the chlorine activation and hence, meteorology of the winters.

The very cold winter 2006 exhibits an extended period of loss rates of about 4 ppbv sh^{-1} until early October, while the winter 2009 shows the shortest span of high loss rates, only until mid-August. The colder winter 2008 also exhibits high loss rates in most months, May–August in particular. In some winters (e.g. 2004 and 2008) the loss rates in August are also higher than those in September. The lidar measurements of Godin et al. (2001) in the Antarctic winters 1992–1998, and model studies of Tripathi et al. (2007) and Frieler et al. (2007) in the Antarctic winter 2003 also show com-

ACPD
14, 28203–28230, 2014

parable loss rates at 475 K. Our analyses are consistent with the loss rates found in the very cold Arctic winters (1994/1995, 1999/2000, 2004/2005, 2010/2011) during the peak loss rate period in January–February, for which loss rates of about 5–8 ppbv sh^{-1} around 450–500 K are estimated (Kuttippurath et al., 2012, 2010; Frieler et al., 2007). No significant ozone production is found at this altitude level.

At 675 K, large interannual variability is found in the ozone loss rates from June to August, which are about 2–5 ppbv sh^{-1}, depending on day of year and winter. The loss rates are typically about 2 ppbv sh^{-1} in September and then increase rapidly to 4–6 ppbv sh^{-1} thereafter. For instance: in 2005, the largest ozone loss rates of 3–5 ppbv sh^{-1} are simulated in early winter, whereas about 3 ppbv sh^{-1} is calculated in 2008. The lowest loss rates among the ten winters during the ozone hole period (June–September) are found in the warm winters of 2010 and 2012, about 1–2 ppbv sh^{-1}. Note that a similar range of loss rates of 2–7 ppbv sh^{-1} is also calculated for the colder Arctic winters in late March and mid- to late April in 2010/2011, February–March in 2008/2009 and March in 2004/2005, depending on day of year (Kuttippurath et al., 2010, 2012).

The production rates at 675 K show large variations from one year to the other, from zero in mid-August to 7 ppbv sh^{-1} in late October. These substantial production rates in the September–October period offset the large loss rates during the same period. The high production rates at the end of winter are expected as small disturbances (toward the final warming) shift the polar vortices to sunlit parts of the mid-latitudes. The analyses on the ozone production and loss rates at 675 K imply that the ozone loss in the middle stratosphere also depends on the position of the polar vortex in the sunlight and the dynamics of the winter.

4 Conclusions

The interannual variability in the Antarctic winter meteorology was relatively large in the last decade, as it consisted of one of the coldest winters (2006), three relatively

ACPD
14, 28203–28230, 2014

warm winters (2004, 2010, and 2012), and three very cold winters (2005, 2008, and 2011). As analyzed from the average of the ten winter simulations, ozone loss in the Antarctic starts at the edge of the vortex at low EqLs (65–67° EqL) by mid-June, consistent with the findings of Lee et al. (2000). Ozone loss progresses with time and advances to higher EqLs (69–83° EqL), with the largest loss at lower EqLs (65–69° EqL) in June–August in agreement with the exposure of the vortex to sunlight. The maximum ozone loss is attained in the mid-September to mid-October period. The peak ozone loss (> 2 ppmv) is found over a broad altitude range of 475–550 K. The maximum modeled ozone loss is about 3.5 ppmv around 550 K in 2005 and 2006, the coldest winters with the largest loss. In contrast, the maximum loss in the warmer winters of 2004, 2010 and 2012 was restricted to 2.6 ppmv. The modeled column loss shows the largest value of 173 DU in 2005 and the lowest of 110 DU in 2004 over 350–850 K, consistent with the meteorology of the winters. The comparison between simulated and observed trace gas evolution during the winters suggests that the diabatic descent during spring is relatively slower in the model and hence, the model underestimates the measured ClO and ozone.

In the lower stratosphere at 500 K, the ozone loss rates have a comparable distribution in all winters, about 2–3 ppbv sh^{-1} in July and 4–5 ppbv sh^{-1} from August to late-September. However, as expected, the very cold winters are characterized by slightly larger and extended periods of high loss rates. In the middle stratosphere at 675 K, a loss rate of about 2–5 ppbv sh^{-1} in July–September, and a production rate of about 4–9 ppbv sh^{-1} in September–October, are simulated. Therefore, these higher production rates largely outweigh the loss rates during the same period.

Our study finds that the halogen cycles ClO–ClO, BrO–ClO, and ClO–O control the Antarctic ozone hole in June–September. Since majority of the Antarctic ozone loss occurs in the lower stratosphere and there are still high levels of anthropogenic ozone depleting substances in the stratosphere, the Antarctic ozone hole will continue to occur for the next few decades and will be dictated by the halogen cycles.

ACPD
14, 28203–28230, 2014

Acknowledgements. The authors would like to thank Cathy Boonne of IPSL/CNRS for the REPROBUS model data. Work at the Jet Propulsion Laboratory, California Institute of Technology, was done under contract to NASA. The ECMWF data are obtained from the NADIR database of NILU and are greatly appreciated. The work is supported by funds from the ANR/ORACLE–O_3 France, the EU SCOUT–O_3 and the FP7 RECONCILE project under the Grant number: RECONCILE-226365-FP7-ENV-2008-1.

References

Burkholder, J. B., Orlando, J. J., and Howard, C. J.: Ultraviolet absorption cross-sections of Cl_2O_2 between 210 and 410 nm, J. Phys. Chem., 94, 687–695, 1990. 28206

Carslaw, K., Luo, B., and Peter, T.: An analytic expression for the composition of aqueous HNO_3–H_2SO_4 stratospheric aerosols including gas phase removal of HNO_3, Geophys. Res. Lett., 22, 1877–1880, doi:10.1029/95GL01668, 1995. 28207

de Laat, A. T. J. and van Weele, M.: The 2010 Antarctic ozone hole: observed reduction in ozone destruction by minor sudden stratospheric warmings, Sci. Rep. 1, 38, doi:10.1038/srep00038, 2011. 28205

Frieler, K., Rex, M., Salawitch, R. J., Canty, T., Streibel, M., Stimpfle, R. M., Pfeilsticker, K., Dorf, M., Weisenstein, D. K., and Godin-Beekmann, S.: Toward a better quantitative understanding of polar stratospheric ozone loss, Geophys. Res. Lett., 33, L10812, doi:10.1029/2005GL025466, 2006. 28215, 28216

Froidevaux, L., Jiang, Y. B., Lambert, A., Livesey, N. J., Read, W. G., Waters, J. W., Browell, E. V., Hair, J. W., Avery, M. A., McGee, T. J., Twigg, L. W., Sumnicht, G. K., Jucks, K. W., Margitan, J. J., Sen, B., Stachnik, R. A., Toon, G. C., Bernath, P. F., Boone, C. D., Walker, K. A., Filipiak, M. J., Harwood, R. S., Fuller, R. A., Manney, G. L., Schwartz, M. J., Daffer, W. H., Drouin, B. J., Cofield, R. E., Cuddy, D. T., Jarnot, R. F., Knosp, B. W., Perun, V. S., Snyder, W. V., Stek, P. C., Thurstans, R. P., and Wagner, P. A.: Validation of Aura Microwave Limb Sounder stratospheric ozone measurements, J. Geophys. Res., 113, D15S20, doi:10.1029/2007JD008771, 2008. 28205, 28207

Godin, S., Bergeret, V., Bekki, S., David, C., Mégie, G.: Study of the interannual ozone loss and the permeability of the Antarctic Polar Vortex from long-term aerosol and ozone lidar

ACPD
14, 28203–28230, 2014

measurements in Dumont d'Urville (66.4° S, 140° E), J. Geophys. Res., 106, 1311–1330, 2001. 28215

Grooß, J.-U., Günther, G., Müller, R., Konopka, P., Bausch, S., Schlager, H., Voigt, C., Volk, C.M., and Toon, G. C.: Simulation of denitrification and ozone loss for the Arctic winter 2002/2003, Atmos. Chem. Phys., 5, 1437–1448, doi:10.5194/acp-5-1437-2005, 2005. 28214

Hanson, D. and Mauersberger, K.: Laboratory studies of the nitric acid trihydrate: implications for the south polar stratosphere, Geophys. Res. Lett., 15, 855–858, 1988. 28206

Hoppel, K., Nedoluha, G., Fromm, M., Allen, D., Bevilacqua, R., Alfred, J., Johnson, B., and König-Langlo, G.: Reduced ozone loss at the upper edge of the Antarctic ozone hole during 2001–2004, Geophys. Res. Lett., 32, L20816, doi:10.1029/2005GL023968, 2005. 28205, 28214

Huck, P. E., Tilmes, S., Bodeker, G. E., Randel, W. J., McDonald, A. J., and Nakajima, H.: An improved measure of ozone depletion in the Antarctic stratosphere, J. Geophys. Res., 112, D11104, doi:10.1029/2006JD007860, 2007. 28205, 28215

Kuttippurath, J., Godin-Beekmann, S., Lefèvre, F., and Goutail, F.: Spatial, temporal, and vertical variability of polar stratospheric ozone loss in the Arctic winters 2004/2005–2009/2010, Atmos. Chem. Phys., 10, 9915–9930, doi:10.5194/acp-10-9915-2010, 2010. 28206, 28211, 28214, 28216

Kuttippurath, J., Godin-Beekmann, S., Lefèvre, F., Nikulin, G., Santee, M. L., and Froidevaux, L.: Record-breaking ozone loss in the Arctic winter 2010/2011: comparison with 1996/1997, Atmos. Chem. Phys., 12, 7073–7085, doi:10.5194/acp-12-7073-2012, 2012. 28211, 28214, 28216

Kuttippurath, J., Lefèvre, F., Pommereau, J.-P., Roscoe, H. K., Goutail, F., Pazmiño, A., and Shanklin, J. D.: Antarctic ozone loss in 1979–2010: first sign of ozone recovery, Atmos. Chem. Phys., 13, 1625–1635, doi:10.5194/acp-13-1625-2013, 2013. 28205, 28215

Lee, A. M., Roscoe, H. K., and Oltmans, S.: Model and measurements show Antarctic ozone loss follows edge of polar night, Geophys. Res. Lett., 27, 3845–3848, 2000. 28208, 28217

Lefèvre, F., Brasseur, G. P., Folkins, I., Smith, A. K., and Simon, P.: Chemistry of the 1991/1992 stratospheric winter: three dimensional model simulation, J. Geophys. Res., 99, 8183–8195, 1994. 28206

Lefèvre F., Figarol, F., Carslaw, K. S., and Peter, T.: The 1997 Arctic ozone depletion quantified from three-dimensional model simulations, Geophys. Res. Lett., 25, 2425–2428, 1998. 28207

ACPD
14, 28203–28230, 2014

Lemmen, C., Dameris, M., Müller, R., and Riese, M.: Chemical ozone loss in a chemistry-climate model from 1960 to 1999, Geophys. Res. Lett., 33, L15820, doi:10.1029/2006GL026939, 2006. 28214

Livesey, N. J., Read, W. G., Froidevaux, L., Lambert, A., Manney, G. L., Pumphrey, H. C., Santee, M. L., Schwartz, M. J., Wang, S., Cofeld, R. E., Cuddy, D. T., Fuller, R. A., Jarnot, R. F., Jiang, J. H., Knosp, B. W., Stek, P. C., Wagner, P. A., and Wu, D. L.: Earth Observing System (EOS) Aura Microwave Limb Sounder (MLS) Version 3.3 Level 2 data quality and description document, JPL D-33509, Jet Propulsion Laboratory California Institute of Technology, Pasadena, California, 1–162, 2011. 28207

Murray, F. W.: On the computation of saturation vapour pressure, J. Appl. Meteorol., 6, 203–204, 1967. 28207

Nash, E. R., Newman, P. A., Rosenfield, J. E., and Schoeberl, M. R.: An objective determination of the polar vortex using Ertel's potential vorticity, J. Geophys. Res., 101, 9471–9478, 1996. 28208

Nickolaisen, S. L., Friedl, R. R., and Sander, S. P.: Kinetics and mechanism of the ClO + ClO reaction – pressure and temperature dependences of the bimolecular and termolecular channels and thermal-decomposition of Chlorine Peroxide, J. Phys. Chem., 98, 155–169, 1994. 28211

Papanastasiou, D. K., Papadimitriou, V. C., Fahey, D. W., and Burkholder, J. B.: UV absorption spectrum of the ClO dimer (Cl_2O_2) between 200 and 420 nm, J. Phys. Chem. A, 113, 13711–13726, 2009. 28206

Pitts, M. C., Poole, L. R., and Thomason, L. W.: CALIPSO polar stratospheric cloud observations: second-generation detection algorithm and composition discrimination, Atmos. Chem. Phys., 9, 7577–7589, doi:10.5194/acp-9-7577-2009, 2009. 28210

Pruppacher, H. R. and Klett, J. D.: Microstructure of atmospheric clouds and precipitations, Atmospheric and Oceanographic Sciences Library, 18, 10–73, 2010. 28207

Rex, M., Salawitch, R. J., von der Gathen, P., Harris, N. R. P., Chipperfield, M. P., and Naujokat, B.: Arctic ozone loss and climate change, Geophys. Res. Lett., 31, L04116, doi:10.1029/2003GL018844, 2004. 28214

Roscoe, H. K., Feng, W., Chipperfield, M. P., Trainic, M., and Shuckburgh, E. F.: The existence of the edge region of the Antarctic stratospheric vortex, J. Geophys. Res., 117, D04301, doi:10.1029/2011JD015940, 2012. 28208

ACPD
14, 28203–28230, 2014

Sander, S., Friedl, R. R., Barkern, J., Golden, D., Kurylo, M., Wine, P., Abbat, J., Burkholder, J., Moortgart, C., Huie, R., and Orkin, R. E.: Chemical kinetics and photochemical data for use in atmospheric studies, Technical Report, NASA/JPL Publication, California, USA, 17, 2011. 28206

Santee, M. L., Manney, G. L., Livesey, N. J. J., Froidevaux, L., MacKenzie, I. A., Pumphrey, H. C., Read, W. G., Schwartz, M. J., Waters, J. W., and Harwood, R. S.: Polar processing and development of the 2004 Antarctic ozone hole: first results from MLS on Aura, Geophys. Res. Lett., 32, L12817, doi:10.1029/2005GL022582, 2005. 28205

Santee, M. L., Lambert, A., Read, W. G., Livesey, N. J., Manney, G. L., Cofield, R. E., Cuddy, D. T., Daffer, W. H., Drouin, B. J., Froidevaux, L., Fuller, R . A., Jarnot, R. F., Knosp, B. W., Perun, V. S., Snyder, W. V., Stek, P. C., Thurstans, R. P., Wagner, P. A., Waters, J. W., Connor, B., Urban, J., Murtagh, D., Ricaud, P., Barrett, B., Kleinböhl, A., Kuttippurath, J., Küllmann, H., von Hobe, M., Toon, G. C., and Stachnik, R. A.: Validation of the Aura Microwave Limb Sounder ClO measurements, J. Geophys. Res., 113, D15S22, doi:10.1029/2007JD008762, 2008a. 28205, 28207, 28211

Santee, M., MacKenzie, I. A., Manney, G., Chipperfield, M., Bernath, P. F., Walker, K. A., Boone, C. D., Froidevaux, L., Livesey, N., and Waters, J. W.: A study of stratospheric chlorine partitioning based on new satellite measurements and modeling, J. Geophys. Res., 113, D12307, doi:10.1029/2007JD009057, 2008b, 28205

Santee, M. L., Manney, G. L., Livesey, N. J., Froidevaux, L., Schwartz, M. J., and Read, W. G.: Trace gas evolution in the lowermost stratosphere from Aura Microwave Limb Sounder measurements, J. Geophys. Res., 116, D18306, doi:10.1029/2011JD015590, 2011. 28205, 28207, 28214

Shine, K. P: The middle atmosphere in the absence of dynamical heat fluxes, Q. J. Roy. Meteor. Soc., 113, 8322, 603–633, 1987. 28206

Sonkaew, T., von Savigny, C., Eichmann, K.-U., Weber, M., Rozanov, A., Bovensmann, H., Burrows, J. P., and Grooß, J.-U.: Chemical ozone losses in Arctic and Antarctic polar winter/spring season derived from SCIAMACHY limb measurements 2002–2009, Atmos. Chem. Phys., 13, 1809–1835, doi:10.5194/acp-13-1809-2013, 2013. 28213

Stimpfle, R. M., Wilmouth, D. M., Salawitch, R. J., and Anderson, J. G.: First measurements of ClOOCl in the stratosphere: the coupling of ClOOCl and ClO in the Arctic polar vortex, J. Geophys. Res., 109, D03301, doi:10.1029/2003JD003811, 2004. 28206

ACPD
14, 28203–28230, 2014

Tilmes, S., Müller, R., Engel, A., Rex, M., and Russell, J. M.: Chemical ozone loss in the Arctic and Antarctic stratosphere between 1992 and 2005, Geophys. Res. Lett., 33, L20812, doi:10.1029/2006GL026925, 2006. 28205, 28214

Tripathi, O. P., Godin-Beekmann, S., Lefèvre, F., Pazmino, A., Hauchecorne, A., Chipperfield, M., Feng, W., Millard, G., Rex, M., Streibel, M., and von der Gathen, P.: Comparison of polar ozone loss rates simulated by 1-D and 3-D models with match observations in recent Antarctic and Arctic winters, J. Geophys. Res., 112, D12308, doi:10.1029/2006JD008370, 2007. 28206, 28214, 28215

Tully, M. B., Klekociuk, A. R., Deschamps, L. L., Henderson, S. I., Krummel, P. B., Fraser, P. J., Shanklin, J., Downey, A. H., Gies, H. P., and Javorniczky, J.: The 2007 Antarctic ozone hole, Aust. Meteorol. Mag., 57, 279–298, 2008. 28205

Tully, M. B., Klekociuk, A. R., Alexander, S. P., Dargaville, R. J., Deschamps, L. L., Fraser, P. J., Gies, H. P., Henderson, S. I., Javorniczky, J., Krummel, P. B., Petelina, S. V., Shanklin, J. D., Siddaway, J. M., and Stone, K. A.: The Antarctic ozone hole during 2008 and 2009, Australian Meteorological and Oceanographic Journal, 61, 77–90, 2011. 28205

von Hobe, M., Salawitch, R. J., Canty, T., Keller-Rudek, H., Moortgat, G. K., Grooß, J.-U., Müller, R., and Stroh, F.: Understanding the kinetics of the ClO dimer cycle, Atmos. Chem. Phys., 7, 3055–3069, doi:10.5194/acp-7-3055-2007, 2007. 28211

Waters, J., Read, W., Froidevaux, L., Jarnot, R., Cofield, R., Flower, D., Lau, G., Pickett, H., Santee, M., Wu, D., Boyles, M., Burke, J., Lay, R., Loo, M., Livesey, N., Lungu, T., Manney, G., Nakamura, L., Perun, V., Ridenoure, B., Shippony, Z., Siegel, P., Thurstans, R., Harwood, R., and Filipiak, M.: The UARS and EOS microwave limb sounder experiments, J. Atmos. Sci., 56, 194–218, 1999. 28205

WMO (World Meteorological Organisation): Scientific assessment of ozone depletion: 2010, Global Ozone Research and Monitoring Project-Report No. 51, Geneva, Switzerland, 572 pp., 2011. 28205, 28209, 28210

Yang, E.-S., Cunnold, D. M., Salawitch, R. J., McCormick, M. P., Russell, J., Zawodny III, J. M., Oltmans, S., and Newchurch, M. J.: Attribution of recovery in lower-stratospheric ozone, J. Geophy. Res., 111, D17309, doi:10.1029/2005JD006371, 2006. 28205

ACPD
14, 28203–28230, 2014

Table 1. The five important ozone depleting chemical cycles (1. ClO_x, 2. BrO_x 3. HO_x, 4. ClO–O, and 5. NO_x) in the polar stratosphere. The instantaneous contribution of the cycles to the ozone loss is illustrated in Fig. 2.

Cycle	Chemical Reactions	Rate limit
1	$ClO + ClO + M \rightarrow Cl_2O_2 + M$ $Cl_2O_2 + h\nu \rightarrow ClOO + Cl$ $ClOO + M \rightarrow Cl + O_2 + M$ $2(Cl + O_3 \rightarrow ClO + O_2)$ net: $2O_3 \rightarrow 3O_2$	[ClO] + [ClO]
2	$BrO + ClO \rightarrow Br + ClOO$ $ClOO + M \rightarrow Cl + O_2 + M$ $Cl + O_3 \rightarrow ClO + O_2$ $Br + O_3 \rightarrow BrO + O_2$ net: $2O_3 \rightarrow 3O_2$	[ClO] + [BrO]
3	$OH + O_3 \rightarrow HO_2 + O_2$ $HO_2 + O_3 \rightarrow OH + 2O_2$ net: $2O_3 \rightarrow 3O_2$	$[HO_2] + [O_3]$
4	$ClO + O \rightarrow Cl + O_2$ $Cl + O_3 \rightarrow ClO + O_2$ net: $O_3 + O \rightarrow 2O_2$	[ClO] + [O]
5	$NO + O_3 \rightarrow NO_2 + O_2$ $NO_2 + O \rightarrow NO + O_2$ net: $O_3 + O \rightarrow 2O_2$	$[NO_2] + [O]$

ACPD
14, 28203–28230, 2014

Table 2. The vortex averaged (defined by ≥ 65° EqL) accumulated partial column ozone loss for the maximum ozone loss period in the Antarctic (25 September to 5 October) in DU estimated over 350–850 K and 400–600 K from the MLS sampling inside the vortex and corresponding Mimosa-Chim simulations interpolated to the observed points (both in space and time) for each winter. The estimated error of the ozone loss from both model results and measurements is about 10 %.

	Ozone Partial Column Loss (DU)									
350–850 K Year	2004	2005	2006	2007	2008	2009	2010	2011	2012	2013
Model	110	173	149	167	156	150	159	155	160	156
MLS	154	166	162	145	143	137	131	135	134	127
400–600 K										
Model	85	114	94	110	108	94	96	106	103	102
MLS	94	108	115	115	99	97	81	97	93	93

ACPD
14, 28203–28230, 2014

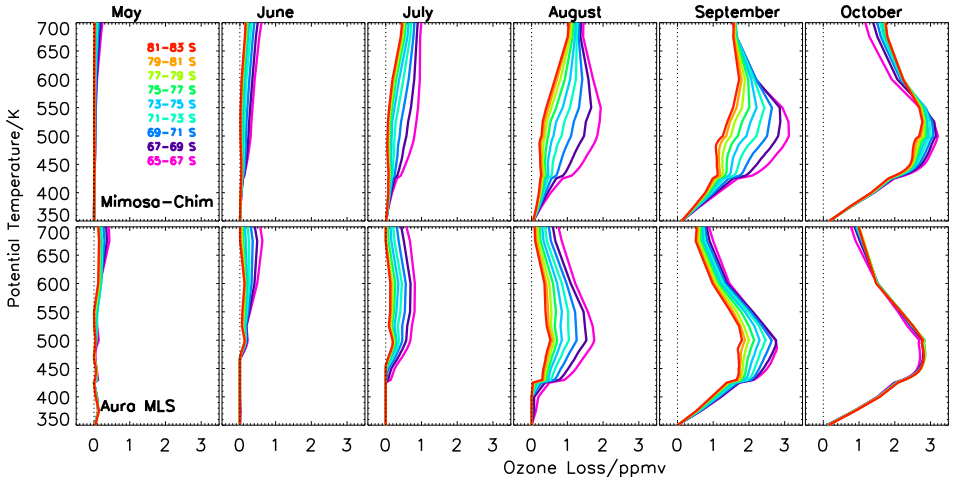

Figure 1. The ten year (2004–2013) average monthly mean ozone loss estimated at different equivalent latitude (EqL) bins (of 2° S) from 65 to 83° S EqL from Mimosa-Chim simulations and the MLS measurements. The model results are interpolated with respect to the time and location of the MLS observations inside the vortex and then averaged for the corresponding day. The black dotted lines represent 0 ppmv.

ACPD
14, 28203–28230, 2014

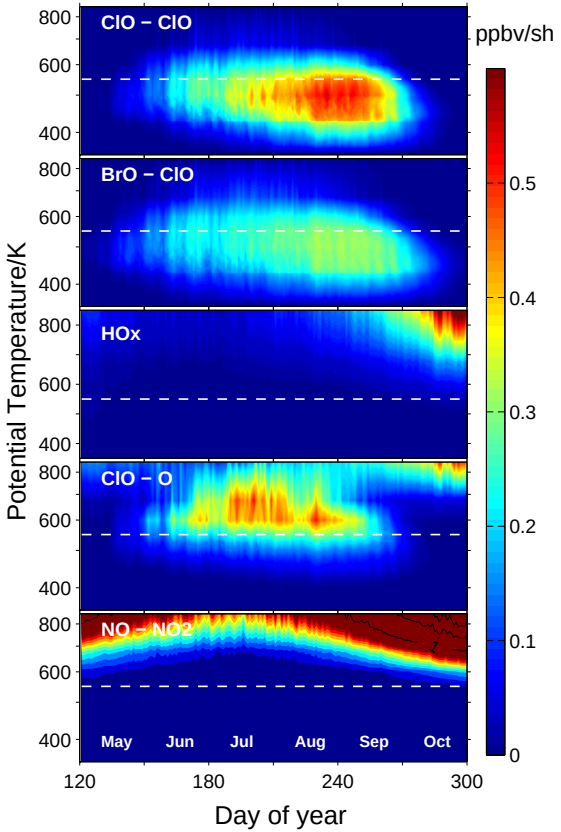

Figure 2. Vortex averaged (defined by ≥ 65° EqL) instantaneous contribution of the five important ozone loss chemical cycles for the (average of) ten Antarctic winters 2004–2013 simulated by the Mimosa-Chim model. The white dashed-lines represent 550 K. Further details of the chemical cycles are given in Table 1. The *y* axis is in logarithmic scale.

ACPD
14, 28203–28230, 2014

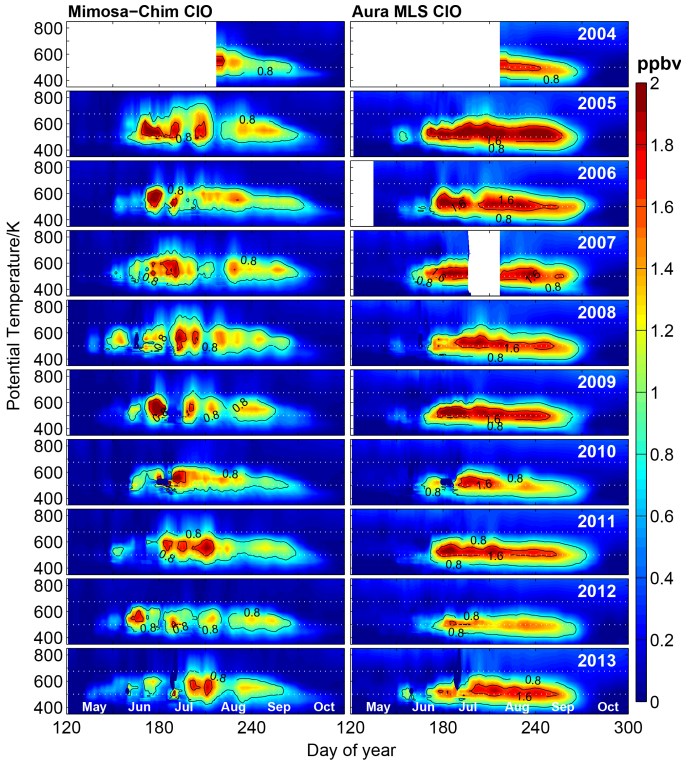

Figure 3. Vertical distribution of the vortex averaged (defined by ≥ 65° EqL) ClO estimated from the Mimosa-Chim model and MLS observations for the Antarctic winters 2004–2013. The model results are interpolated with respect to the time and location of the MLS observations inside the vortex and then averaged for the corresponding day. ClO data are not available during early May 2006 and late July and early August 2007. The measurements are selected with respect to local solar time 10–16 h and solar zenith angles below 89° as available. Both model results and MLS data are smoothed for seven days. The white dotted lines represent 500 and 675 K.

ACPD
14, 28203–28230, 2014

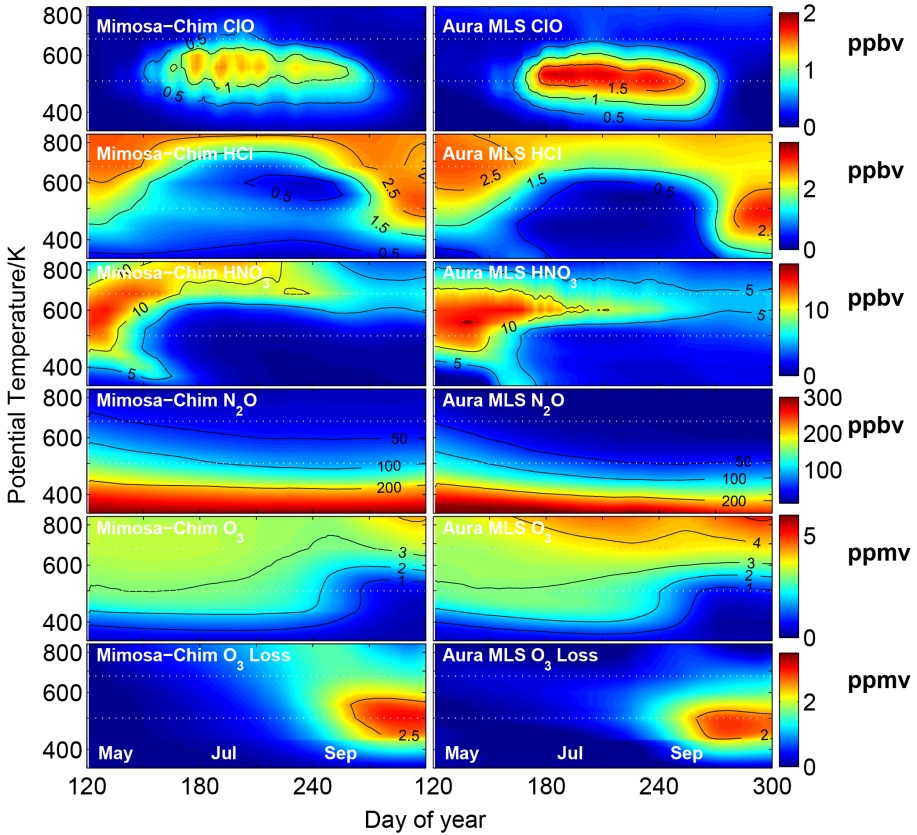

Figure 4. The vortex averaged (defined by ≥ 65° EqL) vertical and temporal evolution of ClO, HCl, N_2O, HNO_3, O_3 and ozone loss from the Mimosa-Chim model and MLS measurements. The model results are interpolated with respect to the time and location of the MLS observations inside the vortex and then averaged for the corresponding time period. The data are the average of ten Antarctic winters in 2004–2013 and are smoothed for 7 days. The vertical axis is in logarithmic scale.

ACPD
14, 28203–28230, 2014

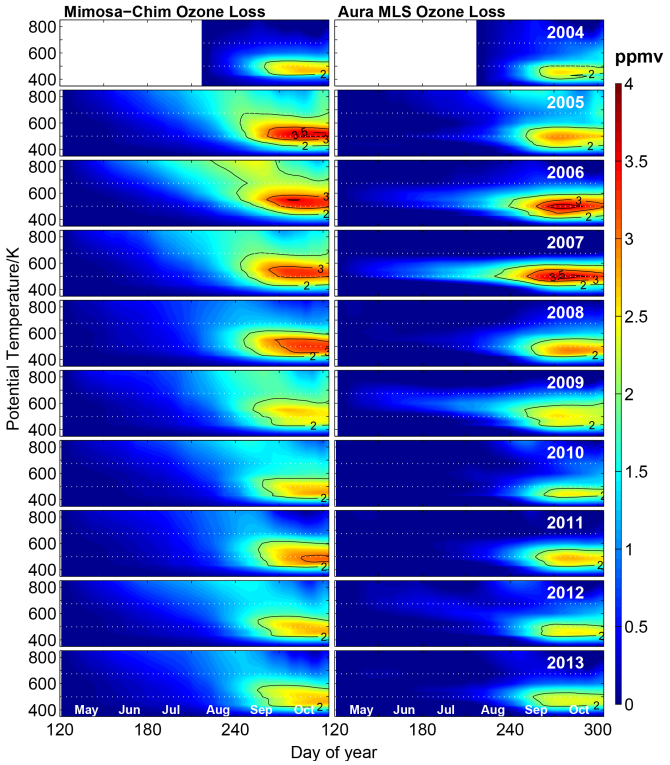

Figure 5. Vertical distribution of the vortex averaged (defined by ≥ 65° EqL) ozone loss estimated for the Antarctic winters 2004–2013. The model results are interpolated with respect to the time and location of the MLS observations inside the vortex and then averaged for the corresponding day. Left: the ozone loss derived from the difference between the passive ozone and the chemically integrated ozone by Mimosa-Chim. Right: the ozone loss derived from the difference between the Mimosa-Chim passive ozone and the ozone measured by MLS. Both model results and MLS data are smoothed for seven days. The white dotted lines represent 500 and 675 K.

ACPD
14, 28203–28230, 2014

Antarctic polar processing and chemistry

J. Kuttippurath et al.

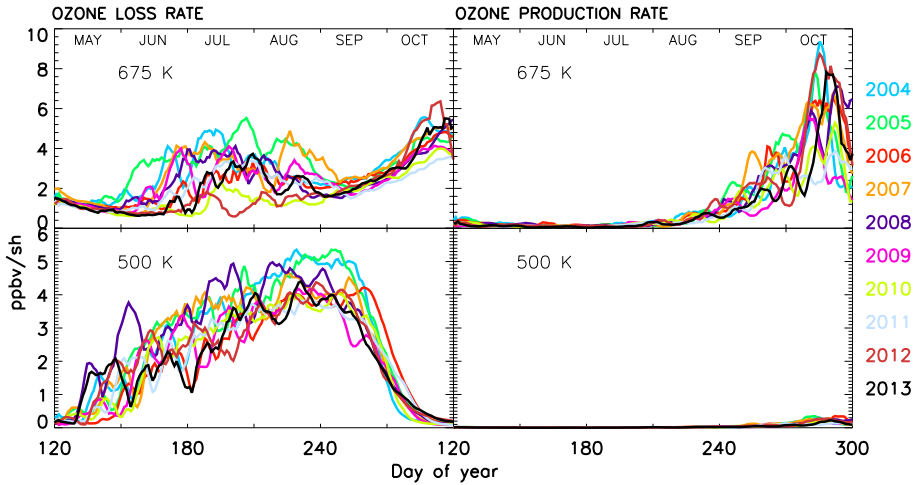

Figure 6. Vortex averaged (defined by ≥ 65° EqL) chemical ozone loss and production rates at 675 and 500 K in ppbv per sunlit hour (ppbv sh^{-1}) for the Antarctic winters 2004–2013 estimated from the Mimosa-Chim model simulations. The data are exempted from temporal smoothing to explicitly show the effect of daily movement of vortex and its impact on ozone production and loss rates.

ACPD
14, 28203–28230, 2014